Slip rate on the low-angle Sevier Desert detachment constrained by geodesy and pluvial shoreline deformation

Nattavadee Srisutthiyakorn

Submitted in partial fulfillment of the requirements for an Honors degree in Geological Sciences from the University of Michigan

26 April 2010

Academic Advisor: Nathan A. Niemi _____

Second Reader: Eric Hetland _____

Table of Contents

ABSTRACT

The conditions that allow slip on low angle normal faults are still on open question, although the existence of low-angle normal faults in the geologic record is generally recognized. In this research project, we analyze the Sevier Desert detachment (SDD) in central Utah for evidence of active slip. Using new geophysical and geologic data that constrain the horizontal and vertical rates of deformation across the Sevier Desert region, we construct an elastic strain model to test whether or not the low-angle Sevier Desert detachment is a viable structure for accommodating 15 ka to recent strain. We derived tectonic vertical surface deformation from the elevations of Bonneville and Provo shorelines after correction for isostatic rebound. Shoreline elevations were digitized from newly released 5 Meter digital elevation models.

We modeled surface deformation due to shear and tensile faults in a half space using Okada (1985), assuming fault geometry constrained by seismic reflection profiles, and varying fault depth, interseismic slip rate, coseismic slip offset, and velocity offset. We show that surface deformation above the SDD can be explained by a half-space fault model with the geometry of the SDD and propose that the detachment is still active. Our best-fit models to the GPS indicate that the SDD is accumulating displacement at a rate of 1.7 ± 0.1 mm/yr and has a locking depth of 7.3 ± 1.4 km. Best-fit models to the deformation of Bonneville and Provo pluvial shorelines indicate a slightly more rapid slip rate over the past ~15 kyrs, in agreement with regional observations of Holocene fault slip rates in the eastern Basin and Range.

1. INTRODUCTION

The mechanisms of formation and slip of low-angle normal faults in the brittle crust is a subject of ongoing controversy (Von Tish et al., 1985; Mitchell and McDonald, 1986; Von Tish et al., 1986; Anders and Christie-Blick, 1994; Wernicke, 1995; Walker et al., 2007; Christie-Blick et al., 2009; Wernicke, 2009). The concept of low-angle normal faults was first introduced by McDonald (1976) through the seismic reflection and the drilling well data of an apparent low-angle structure beneath the Sevier Desert basin. Despite widespread recognition of such structures in the geologic record (Wernicke, 1995; Axen and Bartley, 1997; Axen et al., 2004), the controversy over active slip on low-angle normal faults persists since the mechanisms of slip on such structures of the cannot be explained with traditional models of stress and fault mechanics (Anderson, 1942). Furthermore, there is minimal evidence of major earthquakes from the faults of magnitude 6 or greater on such low-angle structures (Anders and Christie-Blick, 1994; Axen, 2007). Andersonian theory of fault mechanics predicts only steep normal faults (>60°) in the brittle crust and, according to friction failure criterion, normal faults should lock if rotated to <30°, assuming the maximum compressive stress is vertical (Anderson, 1942). If normal faults do slip at shallow dips, a reevaluation of our current understanding of fault mechanics is a necessity (Axen, 2007; Weinberg et al., 2007).

Whether the normal faults initiate at low angles or if they initiate at high angles and are later rotated to lower dips is also an unsolved question. Such rotation of high-angle faults might explain the lack of observed low-angle normal fault mechanisms (Wernicke, 1995). This hypothesis is supported by Spencer (1984), who states that an isostatic mechanism can play a

major role in tilting normal faults. As the hanging wall block slips down, the footwall block then gradually rebounds causing the fault to rotate to shallower dips (Spencer, 1984). Such a scenario would explain the lack of observed low-angle focal mechanisms, and has been incorporated in models of large-magnitude crustal extension (Wernicke and Axen, 1988); however, a clear example of the occurrence of this process is still unknown in the continental crust (Axen and Bartley, 1997). Reduced friction on low-angle normal faults or rotations of the stress field around the fault are other alternatives to explaining their occurrence (Axen, 2007). There is more evidence to support low friction as a cause of fault slip than stress rotation. Reduced fault friction can be achieved by high fluid pressure or weak fault-zone materials (Rice et al., 1992), and may be enhanced by clay minerals which grow authigenically in the fault zone (Solum and van der Pluijm, 2009).

Despite widespread recognition in the geologic record (e.g. Allmendinger et al., 1983), little evidence exists to demonstrate active slip on a low-angle normal fault. Geodetic data suggest that the Alto Tiberina fault in Italy may slip aseismically at dips as shallow as 15° (Abers, 2009; Hreinsdóttir and Bennett, 2009), and that high-angle faults in the eastern Basin and Range may join into a single low-angle (30°) detachment beneath the Great Salt Lake (Velasco et al., 2009). Nonetheless, controversy over the nature and existence of low-angle normal faults continues to persist, with much of the emphasis placed on interpretation of low-angle structures in the western United States, where the concepts of low-angle faulting were first developed (e.g. Armstrong, 1972; Wernicke, 1981). The Sevier Desert detachment in Utah, first recognized in geophysical imaging (McDonald, 1976), has played a central role in these discussions (e.g. Anders and Christie-Blick, 1994; Allmendinger et al., 1995; Anders et al., 1998;

Christie-Blick et al., 2009), in part because any slip on this fault must have occurred at low-angles, and in part because inferences about the nature of the fault are limited to geophysical subsurface imaging and spare borehole cuttings (Anders and Christie-Blick, 1994). The controversy over the nature and origin of the Sevier Desert detachment, combined with excellent geophysical imaging, borehole data, shallow depths to the detachment surface and few issues with land access have led to proposals to drill the detachment in an attempt to better understand the properties that govern slip on low-angle normal faults (Christie-Blick et al., 2009). If the Sevier Desert detachment is currently active, such a scientific borehole would provide significant new insights into the mechanics of low-angle normal faults (Wernicke, 2009).

Here we present new models that bear on the question of whether or not the Sevier Desert detachment is an active normal fault. These models are constrained by a wealth of new geodetic data across the Sevier Desert detachment provided by the Plate Boundary Observatory, and new high-resolution digital elevation models of central Utah that provide the opportunity to resolve tectonic deformation of pluvial shorelines above the Sevier Desert detachment.

2. SEVIER DESERT BASIN

2.1 Brief Geologic History

Our area of study is the Sevier Desert basin in west-central Utah, which is a part of the eastern Basin and Range province. The Basin and Range area extends from southern Oregon to

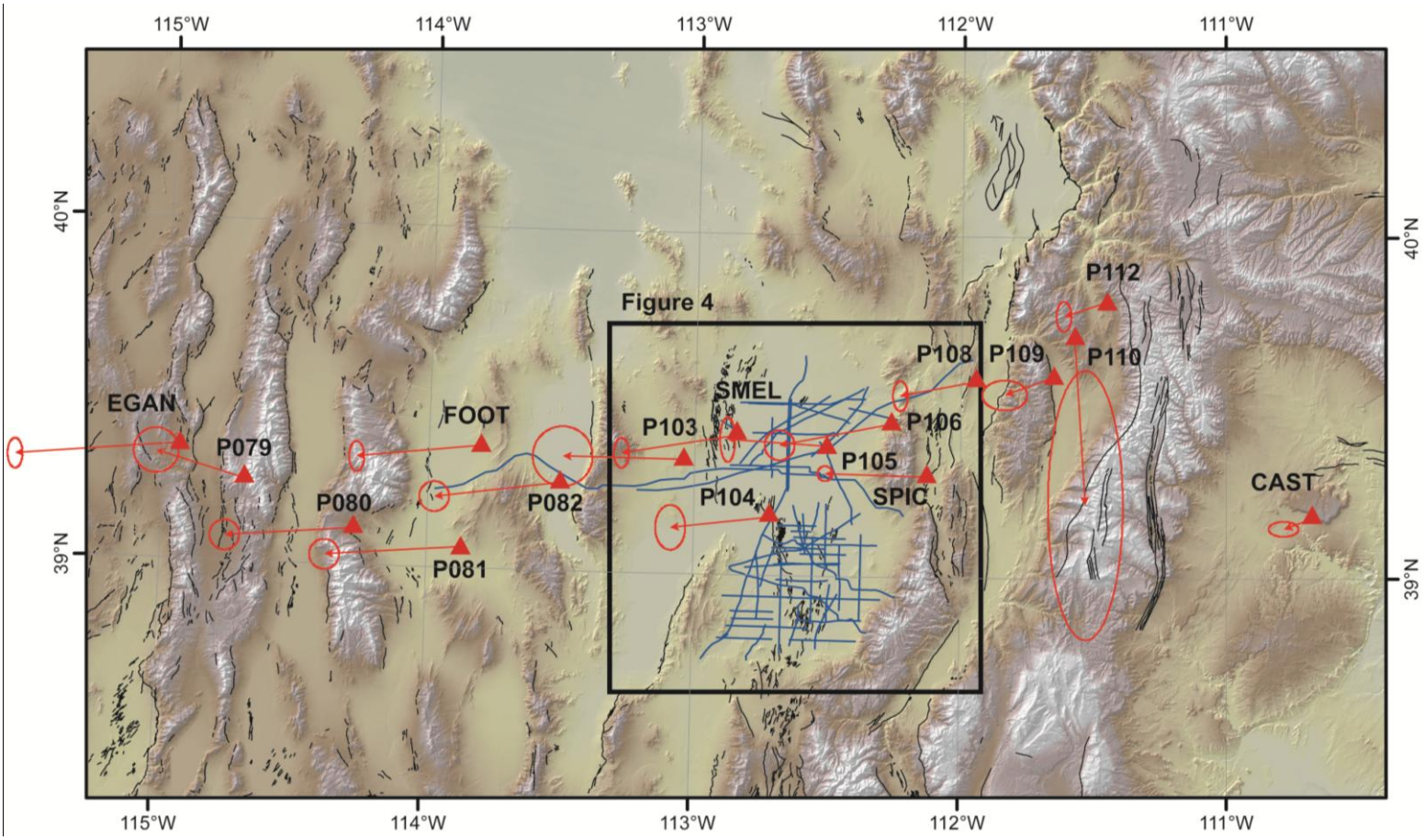

Figure 1. *(A) Eastern Basin and Range shaded relief map showing the GPS stations in red triangles, Seismic reflection profiles in blue lines, and fault scarps in black lines. The black box indicates our study area, the Sevier Desert, and shows the area of Figure 4.*

western Texas and is composed of a series of north-south-trending fault-bounded mountain blocks separated by fluvial basins (Von Tish et al., 1985).

The extensional features underlying the Sevier Desert basin have been seismically imaged over an area of 7,000 km^2, and have been active during middle to late Cenozoic (Fig. 1, Allmendinger et al., 1983; Von Tish et al., 1985). The Cenozoic extension in Sevier Desert took place in two periods. Large movements of the extension occurred during middle Oligocene to Miocene, followed by a short period of quiescence (Stockli et al., 2001). The extension appears

to continue to the present and clearly offsets middle Pliocene basalts (Mitchell and McDonald, 1986).

During the late Pleistocene, Lake Bonneville, the largest non-glacial lake in the western hemisphere, covered the eastern Basin and Range to an area greater than 49,000 km^2 (Passey, 1981). Lake Bonneville began to fill around 25,000 years ago and reached a maximum at the level of the Bonneville shorelines around 15,000 ^{14}C years ago (Oviatt et al., 1992). Shorelines associated with the Provo highstand were formed after Lake Bonneville reached a stable state at around 13,000 ^{14}C years ago (Oviatt et al., 1992). Following the Provo highstand, lake levels again dropped, segmenting the lake into northern and southern bodies. The southern body, called Lake Gunnison, is the precursor to the modern-day Sevier Lake. Throughout the Sevier Desert region, shorelines of the Bonneville and Provo highstands are well-preserved, and record crustal deformation resulting from isostatic rebound (Gilbert, 1890) and neotectonic deformation (Currey, 1982).

2.2 Previous Work

The Sevier Desert detachment is clearly imaged by the Consortium for Continental Reflection Profiling (COCORP) seismic reflection profiles. The COCORP seismic reflection data shows prominent low-angle west-dipping seismic reflections beneath the Sevier Desert. The reflectors can be traced as long as 120 km perpendicular to the strike and as deep as 15-20 km (Allmendinger et al., 1983; Anders and Christie-Blick, 1994). Since there is no evidence of any high-angle normal faults that cut through the Sevier Desert detachment, the detachment must then be the most recent tectonic feature in the area (Allmendinger et al., 1983).

Anders and Christie-Blick (1994) raises the point that the detachment may not be a normal fault because of the lack of evidence in the borehole. Drill cuttings and cores from two industry boreholes (ARCO Hole-in-the-Rock (AHR) and ARCO Meadow Federal #1) do not have any fault-related deformation (Anders and Christie-Blick, 1994). However, some authors argue that lack of evidence in the borehole may be caused by the uncertainties in collecting and interpreting cuttings (Allmendinger et al., 1995). In addition, the absence of indications of brittle deformation does not signify that there is no fault activity. The slip of the fault may be supported by lubrication from mud so that the brittle deformation of grains is unnecessary (Solum and van der Pluijm, 2009).

Based on sparse geodetic data, and comparisons with geologic rates of deformation estimated from paleoseismology, Niemi et al. (2004) proposed that there is active slip on the Sevier Desert detachment. The scarcity of continuous GPS at the time of that study precluded detailed modeling of strain accumulation associated with the Sevier Desert detachment, but geologic estimates of 1.4 mm/yr of slip over the last ~100 kyr were inferred. Here we expand on the neotectonic and geodetic analysis of Niemi et al. (2004) to provide refined estimates of recent activity of the Sevier Desert detachment, incorporating the dense Plate Boundary Observatory GPS velocity field, and high resolution digital elevation models to define tectonic deformation of the Bonneville and Provo shorelines above the Sevier Desert detachment.

3. METHODOLOGY

We compare vertical coseismic deformation constrained by the deformation of Pleistocene shorelines and horizontal interseismic deformation from GPS velocities to surface

deformation predicted by an elastic strain model (Okada, 1985) constrained by the observed geometry of the Sevier Desert detachment (Von Tish et al., 1985). We compare cumulative coseismic offsets to the shorelines, using the elastic dislocation solutions of Okada (1985) and allowing slip from the near surface down to a given locking depth. We compare the predicts interseismic velocities of the elastic strain accumulating model of Savage and Burford (1973), generalized to 3D using the elastic dislocation solution of the Okada (1985), such that interseismic velocities are generated by allowing slip from a given locking depth to infinity.

3.1 Deformation of Pleistocene Bonneville and Provo Shorelines

In this research project, a 5 Meter Digital Elevation Model (5-m DEM) created from autocorrelation of high resolution aerial photographs was employed to create elevation profiles of the Bonneville and Provo highstand shorelines. The shorelines were traced from a 5-m DEM hillshade with geologic maps showing the boundaries of the shorelines as a guide. The elevations of the shorelines were then corrected for isostatic rebound to isolate the tectonic component of shoreline deformation.

3.1.1 Topographic Data Sets

Bonneville and Provo highstand shorelines were digitized from 5 meter digital elevations models available from the state of Utah, and created by the autocorrelation of aerial photographs. These data were the highest resolution available for the Sevier Desert region, but can be compared to other, higher resolution topographic datasets available in metropolitan areas of Utah to assess topographic data accuracy and fidelity. Available digital topographic datasets in Utah include 1-meter Light Detection and Ranging (LIDAR) Digital Elevation Models

(DEMs), 2-meter and 5-meter DEMS from the autocorrelation of aerial photographs, and 20-meter DEMs from interpolation of contour lines (the National Elevation Dataset, NED).

Comparisons of 9 parallel elevation profiles extracted from these four DEM sources from an area located near Weber, Utah (Fig. 2) demonstrate the relative fidelity of each data set. The elevation profiles of 2-m DEM and LIDAR are nearly identical, and 5-m DEM closely resembles to these two topographic data sets (Fig. 3). On the other hand, the elevation profiles extracted from the NED show step-like profiles which are the result of its coarse resolution and derivation from interpolated contour data (Fig. 3). This comparison indicates that the 5-meter DEM, currently the highest resolution dataset available for the Sevier Desert region, is comparable to the highest quality digital elevation models that can currently be produced, and thus should have adequate accuracy and elevation control to constrain shoreline elevations above the Sevier Desert detachment.

3.1.2 Extraction of Shoreline Angles

Using the ArcGIS software package, the shoreline angles of the Bonneville and Provo highstands of Lake Bonnevile were digitized (Fig. 4). We identified ancient shoreline angles using published shorelines from geologic maps, along with abrasion platforms apparent on the Utah 5-m hillshaded DEM. A freely available profiling tool, (Profile Tool v1.2.1, http://arcscripts.esri.com) was used to extract evenly spaced points at 10 meter intervals along all lengths of the digitized shoreline. Elevations at each of these points were determined by using the Utah 5-m digital elevation model.

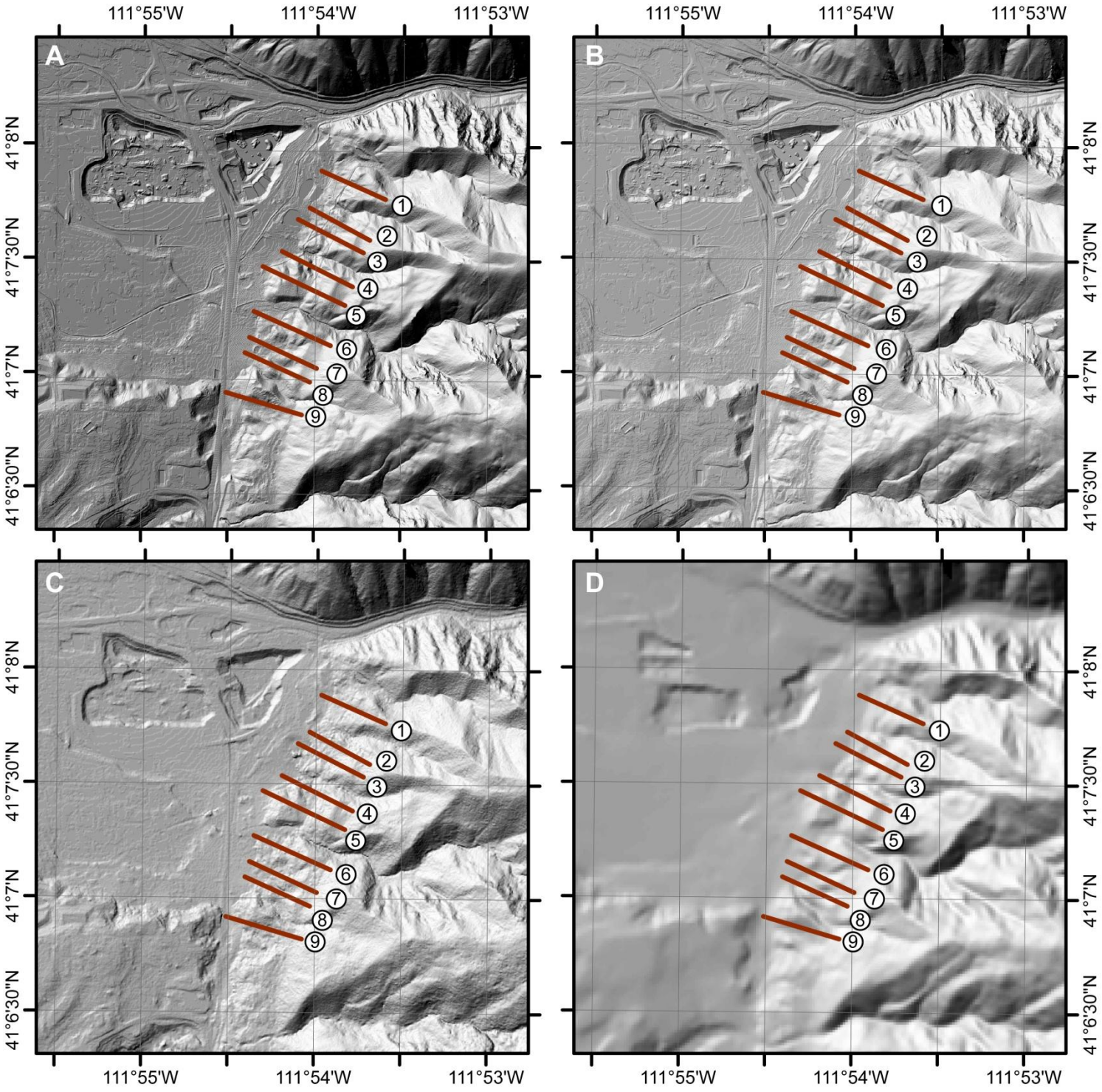

Figure 2. *Shaded relief rendered from (A) 1-m (B) 2-m (C) 5-m and (D) 20-m digital elevation models (DEMs). Resolution of topographic features on DEMs generated from continuous data (1-m LIDAR and 2-m and 5-m auto-correlated aerial photographs) is significantly better than on the 20-m DEM generated from interpolation of contour lines. DEMs in (A), (B), and (C) are from the Utah GIS Portal (http://gis.utah.gov/). DEM in (D) from the National Elevation Dataset (http://ned.usgs.gov). The red lines show the locations of topographic profiles compared in Figure 3.*

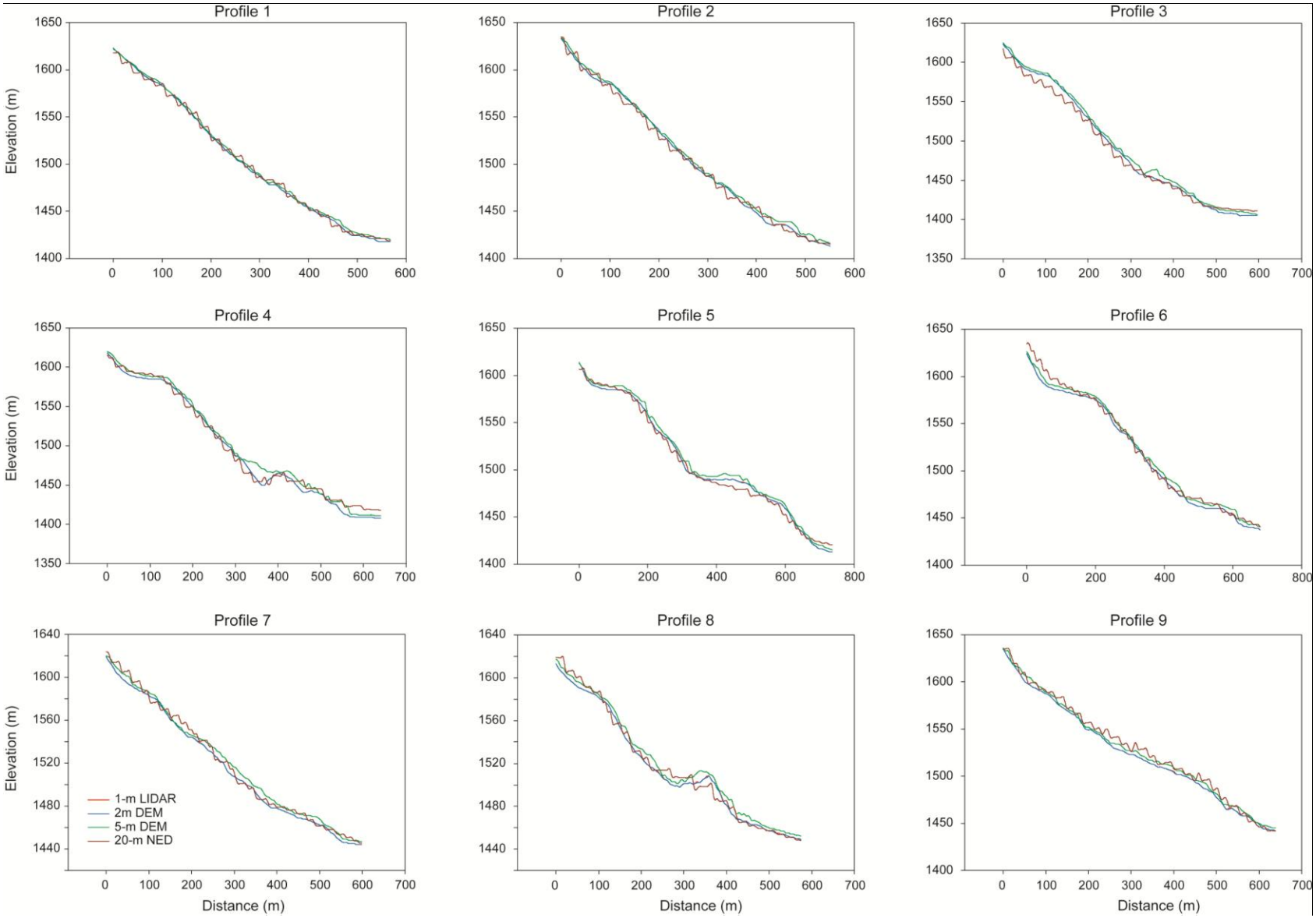

Figure 3. *Nine topographic profiles located near Weber Canyon, Utah. Locations of the profiles are shown on Figure 2. Each panel compares topographic profiles along the same line derived from 1-m LIDAR, 2- and 5-m auto-correlated aerial photograph, and 20-m contour interpolated digital elevation models (DEMs). Topographic profiles extracted from LIDAR and 2-m DEMs are remarkably smooth, and virtually indistinguishable from one another. Topographic profiles from the 20-m interpolated DEM are stair-stepped and artifacts of interpolation are readily apparent. Topographic profiles from 5-m DEMs are smooth, but depart to some extent from the LIDAR and 2-m profiles. These departures are likely due to the across-track averaging of topography.*

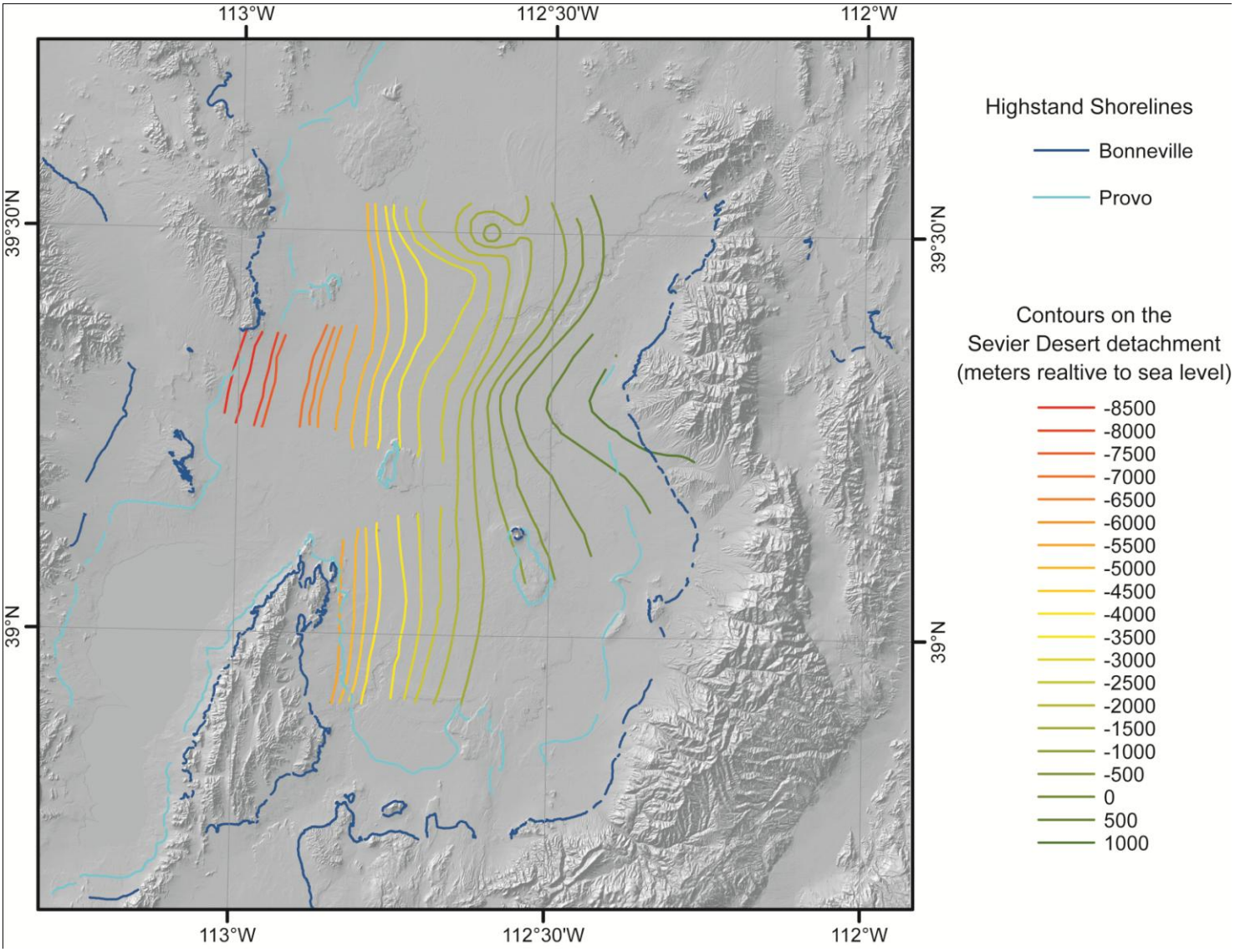

Figure 4. *Hillshaded relief map of the Sevier Desert, rendered from a 5-m DEM, showing extracted Lake Bonneville shoreline angles. The Bonneville highstand is shown in dark blue and the Provo highstand in light blue. The depth contour map of the Sevier Desert detachment is from COCORP seismic reflection profiles (Von Tish et al., 1985), and shows elevation of the detachment surface relative to sea level*

3.1.3 Correction for Isostatic Rebound

The modern elevation of the Bonneville and Provo highstand shorelines is a function of both tectonic deformation (e.g. Currey, 1982) and isostatic rebound resulting from the removal of the load of ancient Lake Bonneville (Gilbert, 1890; Bills et al., 1994). Correction for the

isostatic component of shoreline deformation can be accomplished by employing the adjustment technique of Oviatt et al. (1992):

$$Z_a = Z_r - [(Z_r - 1200)/(Z_b - 1200)][Z_b - 1552]$$

where Z_a is the elevation adjusted for isostatic rebound, Z_r is modern elevation obtained from the 5-m DEM, Z_b is the shoreline altitude at a known point (our data are corrected to points surveyed by Currey (1982) that are nearest to the particular shoreline point to be corrected). This adjustment should result in an isostatically-corrected set of shoreline elevations that reflects solely tectonic deformation of the shorelines.

The shoreline altitude data from Currey was used in the calculation because this data set was comprised independently of any previous study and the measurement of altitude was completed with "standardize set of procedure by a single investigator" (Currey, 1982). Currey reports 181 points of shoreline altitude data from Lake Bonneville and 112 points of shoreline altitude data from Lake Provo (Currey, 1982). This same adjustment was also exercised by Godsey (2005).

3.1.4 Calculating Mean Shoreline Elevations

The full suite of shoreline elevations for both the Bonneville and Provo highstands was subdivided into north-south oriented bins with a width of 10 km. The mean elevation of the shorelines in each bin was calculated, and the standard errors of the shoreline elevations in each bin were determined. These mean shoreline elevations and errors were used as vertical deformation constraints in our elastic deformation model (Fig. 5B).

3.2 Global Positioning System (GPS)

We use Global Positioning System (GPS) data from the Plate Boundary Observatory (PBO) component of the EarthScope project (http://pboweb.unavco.org/). Of the approximately 1,100 permanent GPS sites of 5-50 km spacing across the western United States, We employ GPS data from 17 sites that are in the proximity of Sevier Desert Basin (Figs. 1 and 5A; Table 1).

Table 1. GPS data selected from the site in the proximity of Sevier Desert Basin.

Station	Lat	Lon	Elev	Vn	Ve	Vv	Vne	Vee	Vve	UTM_X	UTM_Y
CAST	39.191022	249.322687	2245.0485	-0.3	-0.8	0.1	0.1	0.2	0.9	527866.776	4338024.44
EGAN	39.345244	245.061146	1998.2756	-0.3	-4.7	-0.9	0.2	0.1	1	160538.518	4362493.88
FOOT	39.369397	246.194627	1547.3893	-0.3	-3.6	0	0.2	0.1	0.9	258326.948	4361524.88
P079	39.25521	245.308343	2746.3622	0.8	-2.5	-2.7	0.3	0.3	1.1	181440.165	4351597.07
P080	39.119439	245.722785	1972.888	-0.2	-3.7	-1.7	0.2	0.2	0.6	216666.122	4335146.65
P081	39.067307	246.128673	1588.1377	-0.2	-3.9	-1.6	0.2	0.2	0.7	251580.891	4328170.56
P082	39.268935	246.494792	1380.9926	-0.4	-3.6	-1.6	0.2	0.2	0.7	283879.41	4349612.98
P103	39.345141	246.957923	1491.3899	0.1	-3.5	-2.2	0.4	0.4	1.7	324027.866	4357066.99
P104	39.186083	247.28288	1397.572	-0.3	-2.9	-1.3	0.3	0.2	0.7	351697.292	4338831.1
P105	39.387544	247.495912	1431.4756	0.2	-2.8	-2.3	0.3	0.1	1.5	370468.92	4360863.2
P106	39.458957	247.737655	1559.5342	-0.6	-3.2	-1.8	0.2	0.2	0.7	391399.307	4368469.92
P108	39.588879	248.055449	1683.2514	-0.4	-2.2	0.6	0.2	0.1	0.6	418891.269	4382554.51
P109	39.597486	248.349167	1760.9659	-0.5	-1.4	-2.6	0.2	0.3	0.8	444120.045	4383285.95
P110	39.715228	248.428858	2266.2112	-4.8	0.3	-0.3	1.8	0.5	1	451045.424	4396307
P112	39.816906	248.550004	1930.3758	-0.4	-1.2	-1.5	0.2	0.1	0.7	461486.01	4407532.74
SMEL	39.425644	247.155072	1422.1484	-0.5	-3.3	0.2	0.2	0.1	0.9	341200.659	4365636.48
SPIC	39.306214	247.872525	1670.4323	0.1	-2.9	-0.6	0.1	0.1	0.5	402790.922	4351364.29

3.3 Inference of Fault Parameters

In this study, we seek to constrain the fault parameters from the paleo-shorelines and GPS data since dislocation skew of Okada (1985) is non-linear with respect to locking depth

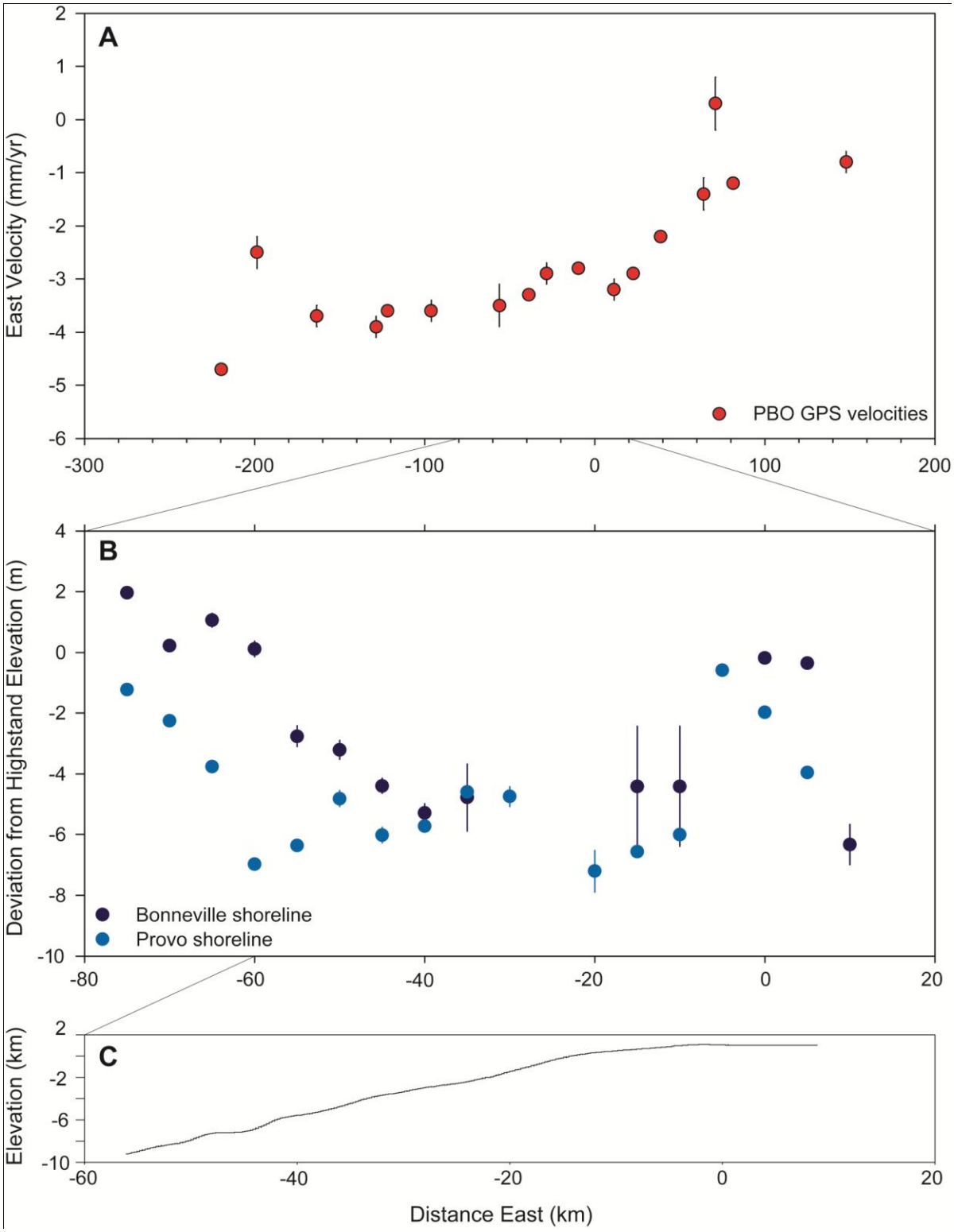

Figure 5. *(A) Plot of GPS east velocities versus distance. (B) Plot of deviation from shoreline elevation for both Bonneville and Provo highstands. Light blue color represents the data set for Provo and dark blue color represents the data set for Bonneville. (C) The trace of Sevier Desert detachment showing the elevation of the detachment with respect to sea level beneath the Sevier Desert basin.*

(km), interseismic slip rate (mm/yr), coseismic slip offset (m), and velocity offset (m). We include a constant velocity offset for the correction to the possibility of strain accumulation on faults that lie further to the east, between the Sevier Desert and the Colorado Plateau (Fig. 1).

We employed a Monte Carlo methodology by randomly generating 10^5 combinations of fault parameters (Table 2). In cases where dense sampling of small values was desired, such as interseismic slip rate and velocity offset, samples were selected from a uniform distribution in log space over an adequate range to cover all reasonable expected values (Table 2). We used MATLAB as our modeling environment, and implemented Okada's (1985) solutions for deformation in a 3D half-space using code developed at the California Institute of Technology. The surface deformation computed from each set of model parameters was compared against our data and the misfits and likelihoods in L1 and L2 norms for each model were calculated.

Specifically, we first compare interseismic strain accumulation modeled by slip on a low-angle detachment to the GPS. We can consider locking depths, which are reasonable for the region, based on the depth of seismicity. We second compare cumulative coseismic displacement on the upper crustal portion of the same low-angle detachment to the Bonneville and Provo highstand shorelines. In the case of the interseismic model, we assume that the slip is occurring continuously from some specified locking depth to infinity (Savage and Burford, 1973). On the other hand, in the coseismic model, we assume that the deformation of the shorelines is the result of cumulative coseismic displacements from earthquakes that is locked during the interseismic period. On the upper portion of the fault, for simplicity, we treat all deformation in two-dimensions, assuming that the Sevier Desert detachment has no strike-slip

motion. We also assume a known geometry of the detachment based on seismic reflection data, using a strike of 0°N and a dip of 15° W. We treat the problem in two-dimensions and project both observations of shoreline deformation and the east components of GPS velocity onto a single east-west profile at latitude 39.25°N.

Table 2. Summary of the range of values used to randomly generate model parameters.

	Variables	Minimum Value	Maximum Value
Vertical Surface Deformation	Locking Depth	0 km	100 km
	Coseismic Slip Offset	0 m	100 m
Horizontal Surface Deformation	Locking Depth (Generated in log space)	10^{-1} km (0.1 km)	$10^{1.7}$ km (50 km)
	Interseismic Slip Rate (Generated in log space)	10^{-1} mm/yr (0.1 mm/yr)	10^{1} mm/yr (10 mm/yr)
	Velocity Offset (Generated in log space)	10^{-1} mm/yr (0.1 mm/yr)	10^{1} mm/yr (10 mm/yr)

The misfits of each model were calculated using both L1-norm and L2-norm, accounting for data error. Misfit calculations for L1-norm were divided into two cases. In the first case we treated the formal errors on the GPS measurements as the full errors, and in the second we increased the values of standard deviation to account for unknown errors in the measurements (e.g. Hammond and Thatcher, 2004). The equations for L1-norm and L2-norm are as followed:

$$L_1 = \sum_{i=1}^{N} \frac{\left|\widehat{d}_i - d_i\right|}{\sigma_i} \qquad L_2^2 = \sum_{i=1}^{N} \frac{\left(\widehat{d}_i - d_i\right)^2}{{\sigma_i}^2}$$

where N is the total number of data, $\widehat{d}_i - d_i$ is the difference between the data and the model, and σ_i is the standard deviation of the data. The error distribution of L1-norm misfit follows a Laplacian error distribution and the L2-norm misfit follows a Gaussian error distribution. Based on the L1 misfit, we compute a relative likelihood using the formula $e^{-(\text{L1 misfit})}$, normalized by the maximum value of likelihood found in the full range of model runs.

4. RESULTS

We expect the solutions for a complex non-linear inverse problem to be poorly constrained. We chose to report the results from the L1-norm adjusted for unmodeled data error since many predictions from our model do not fit the 95% confidence level of our observational data. A summary of these results can be found in Table 3.

For the usual model ensemble, the likelihood was randomly retained. As an example, for models that had a likelihood value of 0.1, only 10% of the models were retained. This process greatly reduced the number of unfit models and the value of the quantile that resulted in the best-fit case would be much lower. However, due to the nature of our observational data, this approach was not applicable, since our calculated misfit values were too high resulting in small values of likelihood.

Therefore, instead of following this technique, we searched for the best-fit model by determining the cutoff threshold for the quantile of relative likelihood. Although defining the cutoff threshold is a subjective quantification, we thought that this would be a better way to approach the solution of the physical system since there is high variability in our observational data. The distribution of likelihood is strongly left skewed as many of the models do not fit properly.

4.1 Best-fit Models for Horizontal Surface Deformation

In order to present how the misfit varies with the four model parameters, we only present model corresponds to the high likelihood velocity offset (Fig. 6). By binning the model

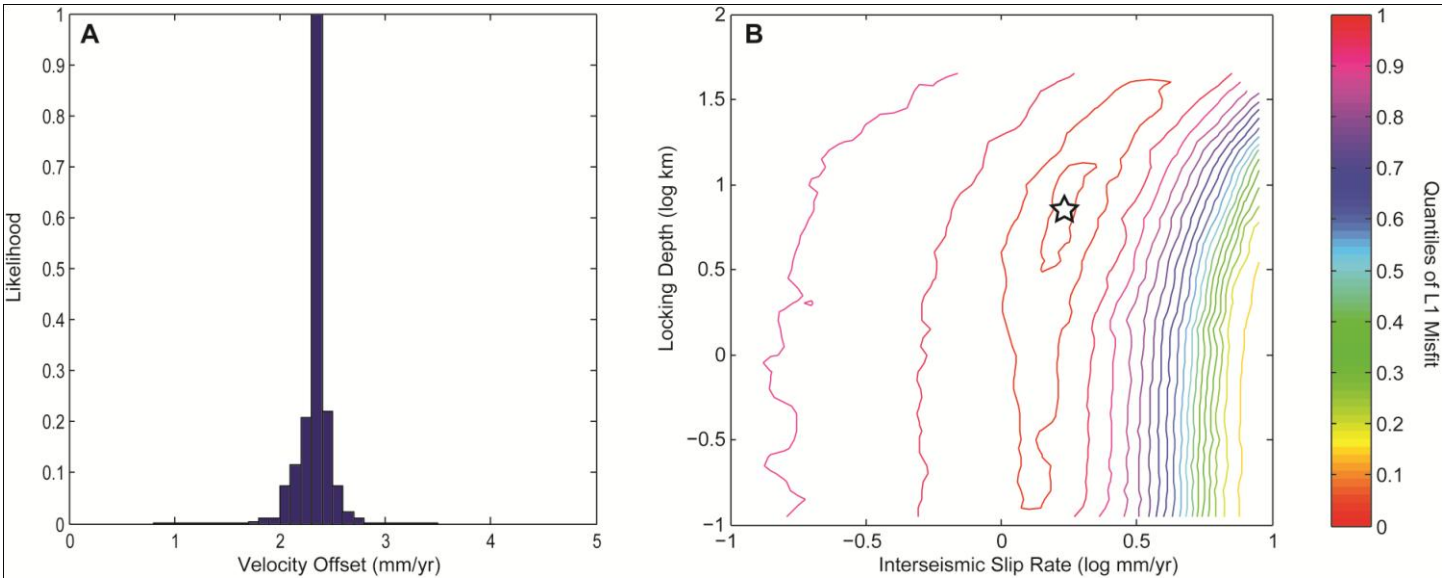

Figure 6. *(A) Histogram of relative likelihood as a function of velocity offset for elastic strain assimilation models. Models with the greatest likelihood of fitting the GPS data have velocities partitioned such that 2.3 to 2.4 mm/yr of westward motion relative to North America is accommodated east of the Sevier Desert. (B) Contours of likelihood quantiles for all models with velocity offsets from 2.3 to 2.4 mm/yr. The star depicts the model with the highest relative likelihood. A plot of the best-fit model against the geodetic data is shown in Figure 8.*

results in 0.1 mm/yr bins on velocity offset, we find that the best-fit models lie in the velocity offset range of 2.3 to 2.4 mm/yr (Fig. 6A). We thus show likelihood as a function of locking depth and slip rate over this velocity offset range shows an elliptical shape, indicating that there are some tradeoffs between the locking depth and interseismic slip rate (Fig. 6B). The major axis of the elliptical shape of the likelihood contours is almost parallel to locking depth, indicating that interseismic slip rate is significantly better constrained than locking depth for these models. The best-fit model parameters are for a locking depth of 7.3 km, an interseismic slip rate of 1.7 mm/yr, and a velocity offset of 2.3 mm/yr (Fig. 7B).

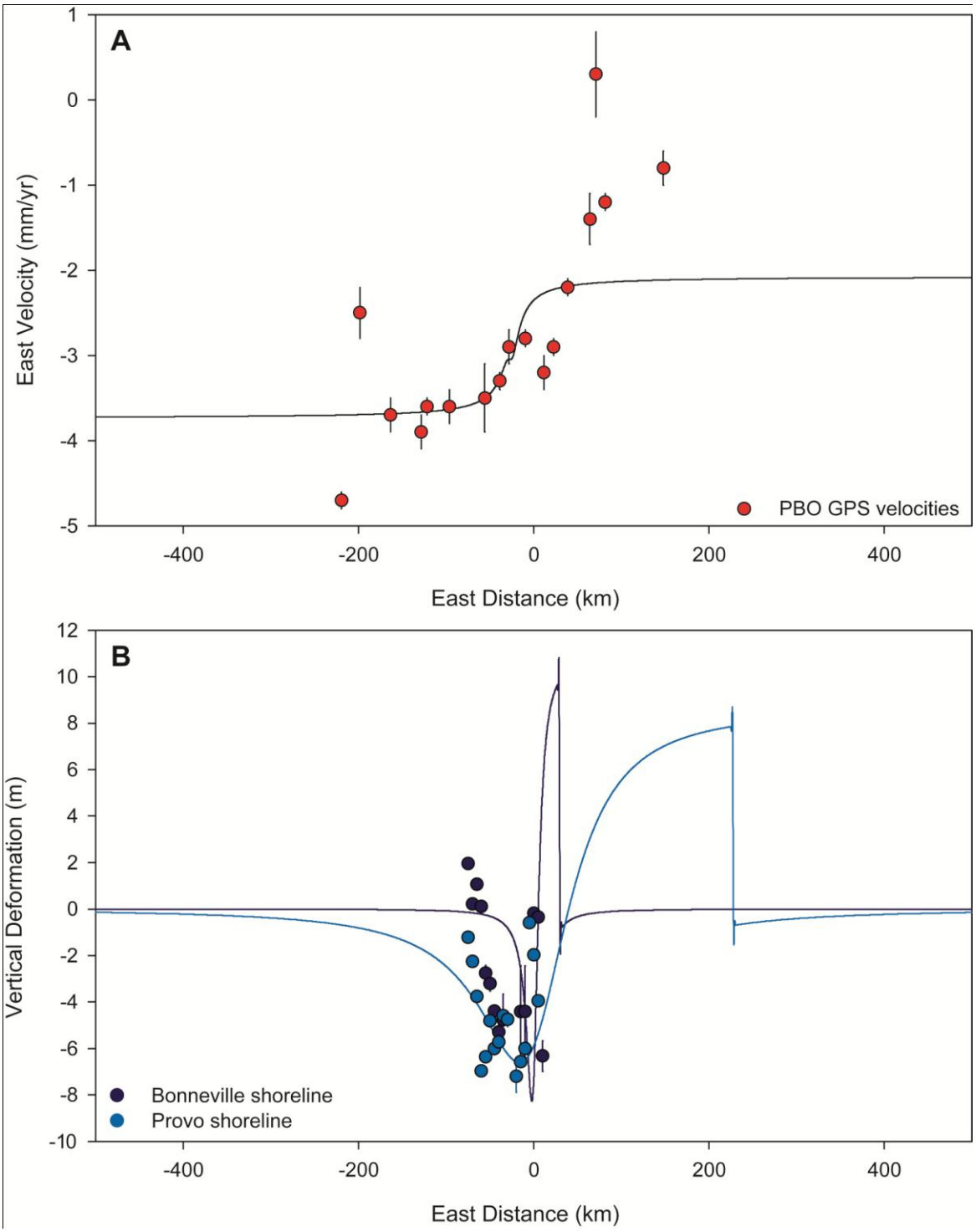

Figure 7. *(A) Best fit elastic strain field model velocities plotted against observed geodetic velocities. (B) Best fit vertical surface deformation models from elastic strain model plotted against observed shoreline deformation data for Bonneville (dark blue) and Provo (light blue) shoreline elevations. The east distance is in km where zero corresponds to the UTM 11N grid coordinate of 380,000 m, the updip surface coordinate of the projected Sevier Desert detacehment.*

Table 3. Mean with standard error for each best-fit model from 10^5 set of model parameters*

Interseismic strain field (Horizontal Deformation)	Locking Depth (km)	Interseismic Slip Rate (mm/yr)	Velocity Offset (mm/yr)
GPS	7.3 ± 1.4	1.7 ± 0.1	2.3 ± 0.04
Coseismic strain field (Vertical Deformation)	**Locking Depth (km)**	**Coseismic Slip Offset (m)**	
Bonneville Shoreline	8.1± 0.02	38.5 ± 1.8	
Provo Shoreline	60.9 ± 0.3	33.0 ± 0.1	

*reported using quantile of 99.99%

4.2 Best-fit Models for Vertical Surface Deformation

We only vary fault locking depth and coseismic offset in the model compared to the vertical deformation, and we show the likelihood function of locking depth and coseismic slip offset (Fig. 8). We have two observational dataset to compare with this model of vertical surface deformation, the deformation of the Bonneville and Provo shorelines. The values of

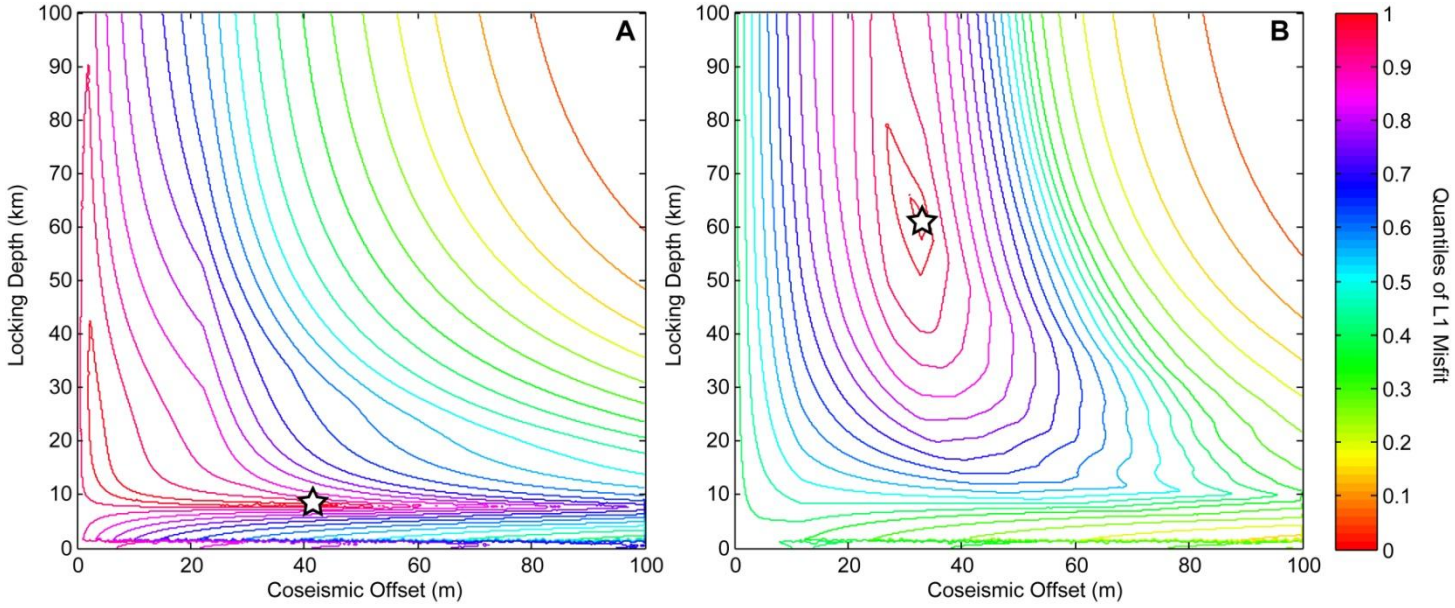

Figure 8. *Contours of likelihood quantiles for models of coseismic deformation of (A) Bonneville and (B) Provo highstand shorelines. On each plot, the star depicts the model with the highest likelihood. Plots of the best-fit models against shoreline deformation data are shown in Figure 7.*

best fit locking depth and cumulative coseismic offset for the Bonneville shorelines are of 8.1 km and 38.5 m, respectively (Fig. 8A). The locking depth is constrained by our models to be fairly shallow. For Provo shorelines, the model parameters with likelihood contour form an elliptical shape, with a clearly defined maximum fit with fairly well constrained locking depth and coseismic offset. The best-fit model show the locking depth of 60.9 km and a coseismic slip offset of 33.0 m (Fig. 7A).

5. DISCUSSION

5.1 INTERSEISMIC STRAIN ACCUMULATION

From the interseismic velocities inferred from continuous GPS, we want to understand whether the modern deformation is localized in the Intermountain Seismic Belt (ISB) along the Wasatch fault (Dixon et al., 1995; Martinez et al., 1998; Thatcher et al., 1999; Dixon et al., 2000), or if it is distributed or structures further to the east (Bennett et al., 1999). Niemi et al. (2004) first detailed the discussion of sparse continuous GPS across the Sevier Desert detachment. They argued for distributed deformation across the eastern Basin and Range, with the majority of slip accommodated on the Sevier Desert detachment (Niemi et al., 2004). Our results for the current slip rate on the Sevier Desert detachment is 1.7 ± 0.1 mm/yr, with 2.3 mm/yr of the geodetic velocity field accommodated on structures further to the east. This represents a 43% to 57% partitioning of strain between the Sevier Desert detachment and presumably the Wasatch fault, suggesting the both are equally responsible for accommodating deformation at this latitude, and contradicting models that localize all deformation at this

latitude onto the Wasatch fault. These results leverage the increased spatial and temporal coverage of geodetic observations from the Plate Boundary Observatory. Prior attempts to estimate slip rates on the Sevier Desert detachment suffered from the sparse coverage of continuous GPS data, for which the spacing of geodetic stations may have been too broad (>100 km) to identify localized strain (Hreinsdóttir and Bennett, 2009).

The slip rate derived above also corroborates the slip rate estimates of both Von Tish et al (1985), who estimated a slip rate of 0.4 to 1.9 mm/yr and Niemi et al. (2004), who estimated a slip rate of 1.4 mm/yr, both on the basis of geologic constraints. The locking depth inferred from GPS data is in accordance with the observed limit of the depth of the fault from COCORP seismic reflection profile as reported by Allmendinger et al. (1983), and is coincident with the observed depth of seismicity in this region (Sibson, 1982). We conclude that the fixed geometry of the Sevier Desert detachment yields reasonable locking depths and slip rates, while fitting the observed GPS velocity constraints, and thus suggests that active slip on this structure is a reasonable hypothesis.

5.2 Locking depth variations between Bonneville and Provo shorelines

From the best-fit models for vertical deformation of pluvial shorelines, we find the value of locking depth inferred from the Bonneville shoreline to be 8.1 ± 0.02 km and from the Provo shoreline to be 60.9 ± 0.3 km. We suspect that the difference in locking depth may be the result of an imperfect adjustment of isostatic rebound for the Provo shoreline. The calendar ages of the Bonneville and Provo shorelines remain an open question, changing with refinements of the ^{14}C age to calendar age calibration (Reimer, 2004). This is important because we want to

determine whether the time between the end of the Bonneville highstand and the beginning of the Provo highstand was long enough to allow fully mantle relaxation (Passey, 1981). New corrections applied to convert ^{14}C ages of the Bonneville and Provo highstands to calendar years (Karow and Hampel, 2009) suggest that the time span between these highstands may be as little as 800 years. Time to attain isostatic equilibrium following lake-level drop from the Bonneville to the Provo shorelines depends on the mantle viscosity underlying the Sevier Desert region, but for most estimates of mantle viscosity, relaxation times are in excess of the 800 years now determined for the time between these two highstands (Crittenden, 1963; Walcott, 1970; Passey, 1981; Bills et al., 1994). If these new ages for the Bonneville and Provo highstands are correct, the Provo shoreline may have developed as a non-equilibrium shoreline, and there may remain an element of long–wavelength deformation in the Provo shoreline elevations that was not removed by our correction for isostatic rebound. The current elevations of the Provo shoreline may then be the result of both isostatic rebound and tectonic deformation above the Sevier Desert detachment. This could potentially account for the deeper locking depth necessary to fit the deformation of the Provo shoreline.

5.3 Holocene Acceleration of Fault Slip

The estimated cumulative coseismic offset of the Bonneville shoreline (38.5 ± 1.8 m) is higher than that of the Provo shoreline (33.0 ± 0.1 m), which is not surprising given that the Bonneville shoreline is older. Assuming that the age of Bonneville highstand is 17,500 years and the age of Provo highstand is 16,700 years, we computed the along-strike slip rates from the

slip offset to be 2.2 mm/yr and 2.0 mm/yr, respectively. These two rates are slightly faster than 1.7 mm/yr rate obtained from continuous GPS data, although perhaps not significantly.

It has previously been noted that faults in the eastern Basin and Range appear to have slipped more rapidly during the Holocene than their time-averaged rates since the Late Pleistocene (Friedrich et al., 2003; Niemi et al., 2004), with such variations in slip rate being ascribed primarily to fault interactions within a complex fault system leading to non-steady strain release. Alternatively, the rapid lowering of Lake Bonneville from the Bonneville to the Provo highstands has been invoked as a mechanism to trigger increased slip on crustal normal faults (Karow and Hampel, 2009). More detailed age and slip rate control are necessary to discriminate between these scenarios, but we note that in order for the Bonneville shoreline to have been deformed by slip on the SDD at an average rate of 2.2 mm/yr since 17.5 ka, while only having been deformed by slip at a rate of 2.0 mm/yr since the Provo highstand at 16.7 ka, the SDD would have had to slip at an exceedingly high rate (~7 mm/yr) over the 700 years between the abandonment of the Bonneville shoreline and the establishment of the Provo shoreline. Such a rapid slip rate is predicted by recent modeling of lake unloading effects on the slip rates of normal faults (Karow and Hampel, 2009).

5.4 Plausibility of Slip on the Sevier Desert Detachment

Our results present remarkable consistency between locking depth and slip rate for elastic deformation due to interseismic strain accumulation recorded by GPS and coseismic deformation of pluvial shorelines given a fixed geometry for the Sevier Desert detachment. This suggests that active slip on this structure is a reasonable hypothesis. The fault is unlikely to

display steady creep since our best-fit models suggest a locking depth of 8 km. If the Sevier Desert detachment displays the steady creep mechanism, we would expect to derive a locking depth closer to the surface instead. One potential explanation for active slip on this fault is a low frictional coefficient (Abers, 2009). This is possible through the incorporation of evaporate into the fault gouge. Such evaporates are observed throughout the Sevier basin (Mitchell and McDonald, 1986). It could also be the case that the stress state at depth near the fault plane is oriented such that the slip is effective and viable (Wernicke, 2009), although determining if this is or is not the case requires *in situ* observations.

6. FUTURE DIRECTIONS

In order to increase accuracy of best-fit models, we will need to increase the number of sets of model parameters. 10^5 sets of model parameters may be inadequate to adequately sample variations in the physical system. We think that at least 10^7 sets of model parameters are required to resolve the physical system and provide a better estimation of the parameters that govern the low-angle normal faults. Our MATLAB codes may need to be rewritten for this purpose.

For further studies, we think that a reevaluation of the shoreline elevations is necessary since the elevation of shorelines may not only be the result from low-angle normal faults. We think that the elevation of shorelines might be affected by other processes, such as volcanic uplift or incomplete correction for isostatic rebound.

7. CONCLUSION

The Sevier Desert detachment is the prime example of a possibly active low-angle normal fault. It can be traced by COCORP seismic reflection profiles in an area covering 7,000 km^2 and extending over 120 km. With the recent availability of high resolution topographic data and higher numbers of GPS stations in Sevier Desert basin, we establish slip rates on this fault with much greater precision than we previously possible (Niemi et al., 2004; Hreinsdóttir and Bennett, 2009).

The slip rate obtained from GPS data supports previous supposition that modern deformation is localized along the Sevier Desert detachment (Niemi et al., 2004) . The slip rates obtained from both shorelines show that it is possible for the fault to slip rapidly due to the regression of Lake Bonneville. The locking depths inferred from GPS data and Bonneville shoreline are in a good agreement and reasonable compared to the depth from seismic reflection profiles. We suspect that unusual high locking depth from the best-models from Provo shoreline may due to long-wavelength deformation of isostatic rebound due to the lack of mantle relaxation time. However, this problem will only be resolved when we know the definite time span of both shorelines.

The Sevier Desert detachment appears to be a third example of an actively slipping low-angle normal fault, with slip rates contrained by geodetic data. This makes this fault an excellent candidate for a scientific drilling study, as has recently been proposed.

ACKNOWLEDGEMENTS

I would like to thank my advisor, Professor Nathan A. Niemi for the guidance and the support he has shown throughout the 3 years I have been involved in this research project and in the writing of this thesis. Without him, I would not have been successful in this endeavor. I would also like to thank Professor Eric A. Hetland for guiding me on solving the inverse problem. Additionally, I would like to thank members of the SCALE lab for their encouragement and advice during this research, especially Alex Lechler for his patience and assistance in teaching me ArcGIS during the entire Summer of 2007.

REFERENCES

Abers, G. A., 2009, Slip on shallow-dipping normal faults: Geology, v. 37, no. 8, p. 767-768.

Allmendinger, R. W., Royse, F., Jr., Anders, M. H., Christie-Blick, N., and Wills, S., 1995, Is the Sevier Desert reflection of west-central Utah a normal fault?: Comment and Reply: Geology, v. 23, no. 7, p. 669-670.

Allmendinger, R. W., Sharp, J. W., Von Tish, D., Serpa, L., Brown, L., Kaufman, S., Oliver, J. E., and Smith, R. B., 1983, Cenozoic and Mesozoic structure of the eastern Basin and Range Province, Utah, from COCORP seismic-reflection data: Geology, v. 11, no. 9, p. 532-536.

Anders, M. H., and Christie-Blick, N., 1994, Is the Sevier Desert reflection of west-central Utah a normal fault?: Geology, v. 22, no. 9, p. 771-774.

Anders, M. H., Christie-Blick, N., Wills, S., Coogan, J. C., and DeCelles, P. G., 1998, Extensional collapse along the Sevier Desert reflection, northern Sevier Desert basin, Western United States; discussion and reply: Geology, v. 26, no. 5, p. 474-475.

Anderson, E. M., 1942, The dynamics of faulting and dyke formation with applications to Britain.

Armstrong, R. L., 1972, Low-Angle (Denudation) Faults, Hinterland of the Sevier Orogenic Belt, Eastern Nevada and Western Utah: Geological Society of America Bulletin, v. 83, no. 6, p. 1729-1754.

Axen, G. J., 2007, Research focus; significance of large-displacement, low-angle normal faults: Geology, v. 35, no. 3, p. 287-288.

Axen, G. J., and Bartley, J. M., 1997, Field tests of rolling hinges: Existence, mechanical types, and implications for extensional tectonics: J. Geophys. Res., v. 102, no. B9, p. 20515-20537.

Axen, G. J., Karner, G. D., Taylor, B., Driscoll, N. W., Kohlstedt, D. L., Morris, J. D., and Silver, E. A., 2004, Mechanics of low-angle normal faults, Rheology and deformation of the lithosphere at continental margins: MARGINS theoretical and experimental earth science series: United States (USA), Columbia University Press, New York, NY, United States (USA).

Bennett, R. A., Davis, J. L., and Wernicke, B. P., 1999, Present-day pattern of Cordilleran deformation in the western United States: Geology, v. 27, no. 4, p. 371-374.

Bennett, R. A., Hreinsdóttir, S., Velasco, M. S., and Fay, N. P., 2007, GPS constraints on vertical crustal motion in the northern Basin and Range: Geophys. Res. Lett., v. 34, no. 22, p. L22319.

Bills, B. G., Currey, D. R., and Marshall, G. A., 1994, Viscosity estimates for the crust and upper mantle from patterns of lacustrine shoreline deformation in the Eastern Great Basin: J. Geophys. Res., v. 99, no. B11, p. 22059-22086.

Christie-Blick, N., Anders, M. H., Manatschal, G., and Wernicke, B. P., 2009, Testing the extensional detachment paradigm; a borehole observatory in the Sevier Desert basin: Scientific Drilling, v. 8, p. 57-59.

Crittenden, M. D., Jr., 1963, New data on the isostatic deformation of Lake Bonneville. Utah: U. S. Geological Survey, Reston, VA, United States (USA), P 0454-E

U. S. Geological Survey Professional Paper.

Currey, D. R., 1982, Lake Bonneville; selected features of relevance to neotectonic analysis: U. S. Geological Survey, Reston, VA, United States (USA), OF 82-1070

Open-File Report - U. S. Geological Survey.

Dixon, T. H., Miller, M., Farina, F., Wang, H., and Johnson, D., 2000, Present-day motion of the Sierra Nevada block and some tectonic implications for the Basin and Range province, North American Cordillera: Tectonics, v. 19, no. 1, p. 1-24.

Dixon, T. H., Robaudo, S., Lee, J., and Reheis, M. C., 1995, Constraints on present-day Basin and Range deformation from space geodesy: Tectonics, v. 14, no. 4, p. 755-772.

Friedrich, A. M., Wernicke, B. P., Niemi, N. A., Bennett, R. A., and Davis, J. L., 2003, Comparison of geodetic and geologic data from the Wasatch region, Utah, and implications for the

spectral character of Earth deformation at periods of 10 to 10 million years: J. Geophys. Res., v. 108, no. B4, p. 2199.

Gilbert, G. K., 1890, Lake Bonneville, Monograph: Reston, VA, U. S. Geological Survey, 438 p.

Godsey, H. S., Currey, D. R., and Chan, M. A., 2005, New evidence for an extended occupation of the Provo shoreline and implications for regional climate change, Pleistocene Lake Bonneville, Utah, USA: Quaternary Research, v. 63, no. 2, p. 212-223.

Hammond, W. C., and Thatcher, W., 2004, Contemporary tectonic deformation of the Basin and Range Province, Western United States; 10 years of observation with the Global Positioning System: Journal of Geophysical Research, v. 109, no. B8, p. 21.

Hreinsdóttir, S., and Bennett, R. A., 2009, Active aseismic creep on the Alto Tiberina low-angle normal fault, Italy: Geology, v. 37, no. 8, p. 683-686.

Karow, T., and Hampel, A., 2009, Slip rate variations on faults in the Basin-and-Range Province caused by regression of Late Pleistocene Lake Bonneville and Lake Lahontan: International Journal of Earth Sciences.

Martinez, L. J., Meertens, C. M., and Smith, R. B., 1998, Rapid deformation rates along the Wasatch Fault Zone, Utah, from first GPS measurements with implications for earthquake hazard: Geophys. Res. Lett., v. 25, no. 4, p. 567-570.

McDonald, R. E., 1976, Tertiary tectonics and sedimentary rocks along the transition: Basin and Range province to plateau and thrust belt province, Utah, *in* Hill, J. G., ed., Symposium on geology of the Cordilleran hingeline, Rocky Mountain Association of Geologists, p. 281-317.

Mitchell, G. C., and McDonald, R. E., 1986, History of Cenozoic extension in central Sevier Desert, west-central Utah, from COCORP seismic reflection data; discussion: AAPG Bulletin, v. 70, no. 8, p. 1015-1021.

Niemi, N. A., Wernicke, B. P., Friedrich, A. M., Simons, M., Bennett, R. A., and Davis, J. L., 2004, BARGEN continuous GPS data across the eastern Basin and Range province, and implications for fault system dynamics: Geophysical Journal International, v. 159, no. 3, p. 842-862.

Okada, Y., 1985, Surface deformation due to shear and tensile faults in a half-space: Bulletin of the Seismological Society of America, v. 75, no. 4, p. 1135-1154.

Oviatt, C. G., Currey, D. R., and Sack, D., 1992, Radiocarbon chronology of Lake Bonneville, Eastern Great Basin, USA: Palaeogeography, Palaeoclimatology, Palaeoecology, v. 99, no. 3-4, p. 225-241.

Passey, Q. R., 1981, Upper mantle viscosity derived from the difference in rebound of the Provo and Bonneville shorelines; Lake Bonneville Basin, Utah: Journal of Geophysical Research, v. 86, no. B12, p. 11,701-11,708.

Reimer, P., 2004, IntCal04 terrestrial radiocarbon age calibration, 0-26 cal kyr BP: Radiocarbon, v. 46, no. 3, p. 1029-1058.

Rice, J. R., Evans, B., and Wong, T.-f., 1992, Fault stress states, pore pressure distributions, and the weakness of the San Andreas Fault, Fault mechanics and transport properties of rocks; a festschrift in honor of W. F. Brace: United States (USA), Acad. Press, San Diego, CA, United States (USA).

Savage, J. C., Burford, R. O. Geodetic Determination of Relative Plate Motion in Central California 1973

Sibson, R. H., 1982, Fault zone models, heat flow, and the depth distribution of earthquakes in the continental crust of the United States: Bulletin of the Seismological Society of America, v. 72, no. 1, p. 151-163.

Solum, J. G., and van der Pluijm, B. A., 2009, Quantification of fabrics in clay gouge from the Carboneras fault, Spain and implications for fault behavior: Tectonophysics, v. 475, no. 3-4, p. 554-562.

Spencer, J. E., 1984, Role of tectonic denudation in warping and uplift of low-angle normal faults: Geology, v. 12, no. 2, p. 95-98.

Stockli, D. F., Linn, J. K., Walker, J. D., and Dumitru, T. A., 2001, Miocene unroofing of the Canyon Range during extension along the Sevier Desert Detachment, west central Utah: Tectonics, v. 20, no. 3, p. 289-307.

Thatcher, W., Foulger, G. R., Julian, B. R., Svarc, J., Quilty, E., and Bawden, G. W., 1999, Present-Day Deformation Across the Basin and Range Province, Western United States: Science, v. 283, no. 5408, p. 1714-1718.

Velasco, M. S., Bennett, R. A., Johnson, R. A., and Hreinsdóttir, S., 2009, Subsurface fault geometries and crustal extension in the eastern Basin and Range Province, western U.S: Tectonophysics, v. In Press, Corrected Proof.

Von Tish, D. B., Allmendinger, R. W., and Sharp, J. W., 1985, History of Cenozoic extension in central Sevier Desert, west-central Utah, from COCORP seismic reflection data: AAPG Bulletin, v. 69, no. 7, p. 1077-1087.

Von Tish, D. B., Allmendinger, R. W., and Sharp, J. W., 1986, History of Cenozoic extension in central Sevier Desert, west-central Utah, from COCORP seismic reflection data; reply: AAPG Bulletin, v. 70, no. 8, p. 1022-1024.

Walcott, R. I., 1970, Flexural Rigidity, Thickness, and Viscosity of the Lithosphere: J. Geophys. Res., v. 75, no. 20, p. 3941-3954.

Walker, C. D., Anders, M. H., and Christie-Blick, N., 2007, Kinematic evidence for downdip movement on the Mormon Peak detachment: Geology, v. 35, no. 3, p. 259-262.

Weinberg, R. F., Regenauer-Lieb, K., and Rosenbaum, G., 2007, Mantle detachment faults and the breakup of cold continental lithosphere: Geology, v. 35, no. 11, p. 1035-1038.

Wernicke, B., 1981, Low-angle normal faults in the Basin and Range Province; nappe tectonics in an extending orogen: Nature (London), v. 291, no. 5817, p. 645-648.

Wernicke, B., 1995, Low-angle normal faults and seismicity; a review: Journal of Geophysical Research, v. 100, no. B10, p. 20,159-20,174.

Wernicke, B., 2009, The detachment era (1977-1982) and its role in revolutionizing continental tectonics; Extending a continent; architecture, rheology and heat budget: Geological Society Special Publications, v. 321, p. 1-8.

Wernicke, B., and Axen, G. J., 1988, On the role of isostasy in the evolution of normal fault systems: Geology, v. 16, no. 9, p. 848-851.